Paramagnetism of caesium titanium alum

Lucjan Dubicki and Mark J. Riley

Citation: The Journal of Chemical Physics **106**, 1669 (1997); doi: 10.1063/1.473320

View online: http://dx.doi.org/10.1063/1.473320

View Table of Contents: http://scitation.aip.org/content/aip/journal/jcp/106/5?ver=pdfcov

Published by the AIP Publishing

Paramagnetism of caesium titanium alum

Lucjan Dubicki
Research School of Chemistry, Australian National University, Canberra, 0200, Australia

Mark J. Riley
Department of Chemistry, University of Queensland, St Lucia, 4072, Australia

(Received 31 May 1996; accepted 16 October 1996)

Caesium titanium alum, $CsTi(SO_4)_2\cdot 12H_2O$, is a β alum and exhibits a large trigonal field and a dynamic Jahn–Teller effect. Exact calculations of the linear $^2T_2\otimes e$ Jahn–Teller coupling show that in the strict S_6 site symmetry the ground multiplet consists of a Kramers doublet $2\Gamma_6$ with magnetic splitting factors $g_\parallel=1.1$ and $g_\perp=0$, a $\Gamma_4\Gamma_5$ doublet at ~ 60 cm^{-1} with $g_\parallel=2.51$ and $g_\perp=0.06$ and another $\Gamma_4\Gamma_5$ doublet at ~ 270 cm^{-1} with $g_\parallel=1.67$ and $g_\perp=1.83$. The controversial g values observed below 4.2 K, $g_\parallel=1.25$ and $g_\perp=1.14$, are shown to arise from low symmetry distortions. These distortions couple the vibronic levels and induce into the ground state the off-diagonal axial Zeeman interaction that exists between the first excited and the ground vibronic levels. © *1997 American Institute of Physics.* [S0021-9606(97)01804-7]

I. INTRODUCTION

Crystals of caesium titanium alum, $CsTi(SO_4)_2\cdot 12H_2O$ (abbreviated as CsTiS), have the cubic space group Pa3 with four equivalent Ti^{3+} ions in the unit cell. The nominally octahedral complex ion, $Ti(H_2O)_6^{3+}$, is slightly compressed along the molecular trigonal axis that lies along one of the body diagonals of the unit cell. The site symmetry at the Ti^{3+} ion is S_6 and the fractional atomic coordinates of the sulphur atoms identify the CsTiS alum to be of the β modification.[1]

The paramagnetism and, in particular, the magnetic g values of CsTiS have been an unresolved problem for more than forty years.[2–7] Unlike the electron paramagnetic resonance (EPR) of Ti^{3+} doped into an α alum such as RbAlS[8] where twelve magnetically inequivalent sites were observed and correspond to one chemical species with rhombic symmetry, the single crystal EPR of CsTiS indicated one chemical species of trigonal symmetry with $g_\parallel=1.25$ and $g_\perp=1.14$.[3] The large linewidth of the EPR lines, about 250 gauss, and the variation of the magnetic susceptibility at low temperatures indicated the presence of low lying paramagnetic states.[3]

If the trigonal field that lifts the degeneracy of the t_2 d-orbitals of the Ti^{3+} ions has a positive sign, $v=E(t_2x_0)-E(t_2x_\pm)$ is greater than zero, then the ground Kramers doublet in S_6 symmetry has the symmetry classification $(t_2x_\pm^1)^2T_2(2\Gamma_6)$ where we use the complex trigonal basis for t_2 orbitals[9] and the double group notation of Koster *et al.*[10]

The $2\Gamma_6$ doublet transforms as the $M_J=\pm\frac{3}{2}$ components of angular momentum $J=\frac{3}{2}$ and has $g_\perp=0$. Indeed, for Ti^{3+} doped in Al_2O_3 where $v=700$ cm^{-1} the observed g values are $g_\parallel=1.07$ and $g_\perp\sim 0.0$.[11] The $g_\parallel$ value differs appreciably from the prediction of the static ligand field model that gives to first order, $g_\parallel(2\Gamma_6)=2-2K_z\approx 0.5$, where K_z is the effective orbital reduction factor for the (t_2^1) $^2T_2$ multiplet. The explanation of this discrepancy as well as accounting for the energies of the low-lying vibronic states at 38 cm^{-1} and 108 cm^{-1} was a major success for Ham's effective Hamiltonian treatment of the $^2T_2\otimes e$ Jahn–Teller problem.[11,12]

Since for positive v the ground state of the Ti^{3+} ion will always remain $2\Gamma_6$ with $g_\perp=0$, the early attempts to account for $g_\perp=1.14$ in CsTiS employed a negative value of v. The $2\Gamma_6$ ground state has $g_\perp=0$ by symmetry, regardless of whether there is Jahn–Teller coupling operating or not. The earlier work culminated in the paper by Shing and Walsh[7] who proposed a $\Gamma_8\otimes e$ Jahn–Teller coupling with a very small trigonal field. This model was based on the assumption that the spin–orbit coupling of the Ti^{3+} ion breaks the $^2T_2(\Gamma_8+\Gamma_7)\otimes e$ coupling into $\Gamma_8\otimes e$ and quenches the pseudo Jahn–Teller coupling between Γ_8 and the higher lying Γ_7, where Γ_8 and Γ_7 are spin–orbit components of $^2T_2$ in the cubic limit. This analysis is not valid because the spin–orbit constant, $\zeta\sim 120$ cm^{-1} in bound Ti(III), is comparable or even less than the Jahn–Teller stabilization energy that has been observed in several Ti^{3+} complexes.[11,13,14]

A new insight into the electronic structure of alums has been revealed by the theoretical work of Daul and Goursot,[15] the electronic Raman measurements of vanadium alums[16] and by more recent x-ray and neutron diffraction structure determinations.[17–20] The work of Best, Forsyth, and Tregenna-Piggott[18–20] have been particularly definitive. All CsMS alums with metal ions having the electronic configuration, (t_2^n) $n<6$, are β alums that are characterized by M(III) ions coordinated by planar water molecules. The OH_2 planes are all rotated about the M–O bonds by $\sim 20°$ with the sense that the oxygen p_π lone pairs normal to the OH_2 plane are tilted towards the trigonal z axis of the $M(OH_2)_6^{3+}$ ion. The structure of CsTiS at 100 K[1] is shown in Fig. 1(a) displaying the S_6 symmetry of the Ti(III) site. The $\sim 20°$ twist of the planar water molecules is midway between the T_h and the ''all horizontal'' D_{3d} symmetries.[19] The angular overlap model shows that such a rotation generates a large positive trigonal field, v.[15]

Consequently, the previous work on CsTiS has focused on the wrong part of the ligand field energy diagram. Since the trigonal splitting of the t_2 orbitals (see Sec. IV) is much greater than the spin–orbit coupling of Ti^{3+} or the Jahn–Teller coupling, it is the trigonal field which tends to break

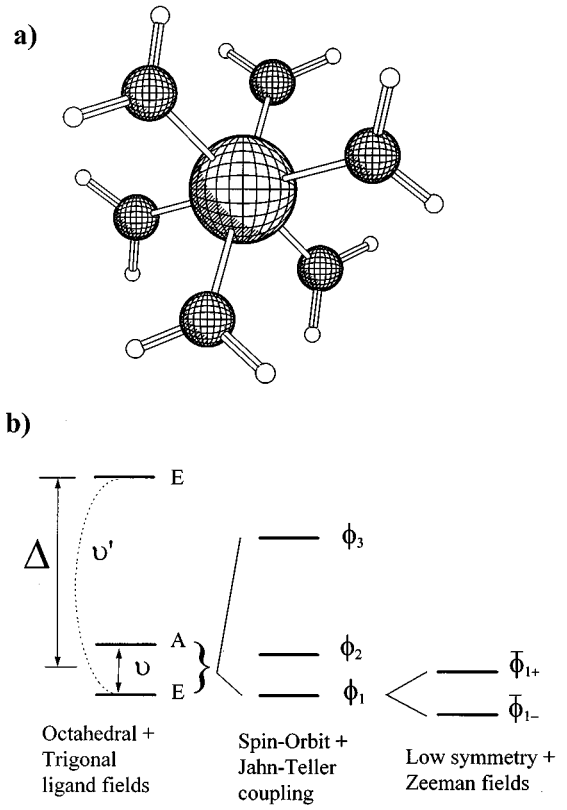

FIG. 1. (a) The S_6 symmetry of the β alum structure viewed down the trigonal axis. (b) A schematic representation of the perturbations acting on the d electronic levels of a Ti(III) ion.

$^2T_2(^2E+^2A)\otimes e$ coupling into $^2E\otimes e$ and ^2A, and quenches the pseudo-Jahn–Teller coupling between ^2E and the higher lying ^2A, where E and A are the trigonal orbital species of the T_2 parent. Figure 1(b) shows a schematic hierarchy of perturbations to the d electronic levels of a Ti(III) complex. These perturbations act simultaneously and are treated as such here. The figure does not imply that a perturbation scheme has been used in this work.

II. $^2T_2\otimes e$ COUPLING IN TRIGONAL SYMMETRY

Since the υ trigonal field in CsTiS is very large (Sec. IV), the vibronic energy levels and the g values will no longer be described accurately by Ham's theory.[12] Instead we diagonalize exactly the $T_2\otimes e$ problem with any trigonal field by using a sufficiently large vibronic basis so that both the calculated energies and g values are independent of the basis size.

The $T_2\otimes e$ Jahn–Teller coupling matrix is given by

$$\begin{array}{c} \\ \langle\xi| \\ \langle\eta| \\ \langle\zeta| \end{array} \begin{array}{c} \begin{array}{ccc} |\xi\rangle & |\eta\rangle & |\zeta\rangle| \end{array} \\ \begin{pmatrix} -\frac{1}{2}Q_x+\frac{\sqrt{3}}{2}Q_y & 0 & 0 \\ 0 & -\frac{1}{2}Q_x-\frac{\sqrt{3}}{2}Q_y & 0 \\ 0 & 0 & Q_x \end{pmatrix} \end{array} \times A_1 \qquad (1)$$

in terms of the real d-orbitals quantized along the cubic axes. Here A_1 is the linear Jahn–Teller coupling constant. It is related to the Jahn–Teller stabilization energy by $E_{JT}=A_1^2/\hbar\omega$ for $T_2\otimes e$ coupling, where $\hbar\omega$ is the wave number of the Jahn–Teller active e vibration. In the complex trigonal basis the coupling matrix becomes

$$\begin{array}{c} \\ \langle\pm\frac{1}{2}X_+| \\ \langle\pm\frac{1}{2}X_-| \\ |\pm\frac{1}{2}X_0| \end{array} \begin{array}{c} \begin{array}{ccc} |\pm\frac{1}{2}X_+\rangle & |\pm\frac{1}{2}X_-\rangle & |\pm\frac{1}{2}X_0\rangle \end{array} \\ \begin{pmatrix} 0 & Q_+ & -Q_- \\ -Q_- & 0 & -Q_+ \\ Q_+ & Q_- & 0 \end{pmatrix} \end{array} \times \sqrt{\tfrac{1}{2}}A_1 \qquad (2)$$

where $Q_\pm=(\mp\sqrt{1/2})(Q_x \pm iQ_y)$ and Q_x, Q_y are the two components of the degenerate e vibration. This Jahn–Teller coupling matrix was included in the 10×10 electronic matrix containing the ligand field and spin–orbit coupling as given by Macfarlane, Wong, and Sturge.[11] Each electronic basis function was then expanded in terms of $n=0,1,2,\ldots,n_v$ levels of a two-dimensional harmonic oscillator vibrational basis. Matrix elements of the Jahn–Teller coupling were then evaluated and the resulting large complex matrix diagonalized. The total basis size without exploiting the vibronic symmetries was $N=10\times\frac{1}{2}\times(n_v+1)(n_v+2)$. A fast Lanczos diagonalization routine for real symmetric matrices was used the find the lowest vibronic energies and wave functions. This meant a further doubling of the size of the original complex matrix. A typical calculation with $n_v=21$ required the diagonalization of a 5060×5060 sparse matrix with 16 148 nonzero off-diagonal matrix elements.

In addition to these calculations, we also used an effective $(t_2^1)^2T_2$ basis corrected for mixing of $(e^1)^2E$ to the second order. By using this electronic basis the vibronic matrix was reduced to $N=3\times\frac{1}{2}\times(n_v+1)(n_v+2)$ as only one component of every Kramers doublet needed to be calculated. The other Kramers component could be generated by performing the time reversal operation. This reduces the computational overhead for $n_v=21$ to the diagonalization of a 1518×1518 real matrix with 5544 nonzero off-diagonal elements. Both types of calculation gave almost identical results.

In both cases, the vibronic levels consist of Kramers doublets, calculated in the absence of an applied magnetic field. The g values were then calculated from evaluating the matrix elements of the Zeeman operator from the zero field eigenfunctions.

For specific cases of near degenerate vibronic levels ($\Delta E<10\ \mathrm{cm}^{-1}$), the off-diagonal Zeeman terms between vibronic levels were also evaluated. The calculations were restricted to linear Jahn–Teller coupling and a single vibrational mode of cubic e symmetry.

In the absence of Jahn–Teller coupling the effective Hamiltonian in the $(t_2^1)^2T_2$ multiplet may be written as

$$\mathbf{H}=-\Delta_t(L_z^2-\tfrac{2}{3})+\sum_\alpha \lambda_\alpha L_\alpha S_\alpha + \sum_\alpha (K_\alpha L_\alpha+2S_\alpha)\mu_B B_\alpha. \qquad (3)$$

The effective ligand field parameters to the second order are

TABLE I. Matrix of the Zeeman Hamiltonian.[a]

	$\|\phi_{1+}\rangle$	$\|\phi_{1-}\rangle$	$\|\phi_{2+}\rangle$	$\|\phi_{2-}\rangle$	$\|\phi_{3+}\rangle$	$\|\phi_{3-}\rangle$
$\langle\phi_{1+}\|$	z_1	z_1'	$x_{12}''-iy_{12}''$	$-x_{12}'-iy_{12}'$	$x_{13}''-iy_{13}''$	$-x_{13}'-iy_{13}'$
$\langle\phi_{1-}\|$		$-z_1$	$x_{12}'-iy_{12}'$	$x_{12}''+iy_{12}''$	$x_{13}'-iy_{13}'$	$x_{13}''+iy_{13}''$
$\langle\phi_{2+}\|$			z_2	x_2-iy_2	z_{23}	$x_{23}-iy_{23}$
$\langle\phi_{2-}\|$				$-z_2$	$x_{23}+iy_{23}$	$-z_{23}$
$\langle\phi_{3+}\|$					z_3	x_3-iy_3
$\langle\phi_{3-}\|$						$-z_3$

[a]The entries α_i or α_{ij} stand for the diagonal, $\frac{1}{2}g_\alpha(\phi_i)\mu_B B_\alpha$, or off-diagonal, $\frac{1}{2}g_\alpha(\phi_i,\phi_j)\mu_B B_\alpha$, matrix elements of the Zeeman operator [Eq. (7)] for the trigonal basis given in Eq. (5). The explicit forms of g_α are given in Table II. All $x_i=y_i$ and $x_{ij}=y_{ij}$.

$$\begin{aligned}
\Delta_t &= \upsilon+(\upsilon')^2/\Delta,\\
\lambda &= \zeta+(\zeta')^2/\Delta,\\
\lambda_z &= \lambda-2\sqrt{2}\zeta'\upsilon'/\Delta,\\
\lambda_x &= \lambda+\sqrt{2}\zeta'\upsilon'/\Delta,\\
K_z &= k-2\sqrt{2}k'\upsilon'/\Delta,\\
K_x &= k+\sqrt{2}k'\upsilon'/\Delta,
\end{aligned} \tag{4}$$

where Δ is the cubic ligand field splitting of the t_2 and e orbitals, υ, ζ and k are the basic one-electron trigonal field, spin–orbit coupling and orbital reduction parameters for t_2 orbitals, respectively, and υ', ζ' and k' are the corresponding set connecting t_2 and e d-orbitals.

The energy levels of the $(t_2^1)^2T_2$ multiplet subject to a Jahn–Teller $T_2\otimes e$ coupling and small υ have been discussed in detail by several authors and will not be reproduced here.[11,21,22] In this paper we will examine more closely the g values of the lowest set of vibronic levels.

For S_6 site symmetry, we use the complex trigonal basis:

$$\begin{aligned}
\phi_{1\pm}(2\Gamma_6) &= |\pm\tfrac{1}{2}X_\pm\rangle,\\
\phi_{2\pm}(\Gamma_4\Gamma_5) &= \cos\theta|\pm\tfrac{1}{2}X_0\rangle+\sin\theta|\mp\tfrac{1}{2}X_\pm\rangle,\\
\phi_{3\pm}(\Gamma_4\Gamma_5) &= \sin\theta|\pm\tfrac{1}{2}X_0\rangle-\cos\theta|\mp\tfrac{1}{2}X_\pm\rangle,
\end{aligned} \tag{5}$$

where $X_\pm$ and X_0 stand for the degenerate and nondegenerate orbital components of the t_2 orbitals, respectively. If υ has a positive sign then the energy order of the three Kramers doublets is $E_1<E_2<E_3$ for both the static ligand field limit and in the presence of linear $T_2\otimes e$ coupling. The angle θ is given by

$$\tan 2\theta=\sqrt{2}\lambda_x/(\tfrac{1}{2}\lambda_z-\Delta_t), \tag{6}$$

which is independent of the Jahn–Teller coupling within Ham's perturbation treatment of the $T_2\otimes e$ model.[23] The accuracy of Eq. (6) should deteriorate as υ becomes large because, as we will show, the transition energies $E_{31}=E_3-E_1$ and $E_{21}=E_2-E_1$ and the g values obtained from an exact calculation progressively deviate from Ham's model.

The second order Zeeman Hamiltonian for a $^2T_2$ multiplet in axial symmetry may be written[9]

$$\begin{aligned}
H(B)=\mu_B\{&g_1\mathbf{S}\cdot\mathbf{B}+g_2[\mathbf{S}\cdot V(E)\cdot\mathbf{B}]\\
&+g_3[\mathbf{S}\cdot V(T_2)\cdot\mathbf{B}]+\mathbf{K}\cdot\mathbf{L}\cdot\mathbf{B}\},
\end{aligned} \tag{7}$$

where the real cubic tensors are normalized as

$$\begin{aligned}
V(Eu) &= 1/\sqrt{6}\ (3L_z^2-2),\\
V(Ev) &= 1/\sqrt{2}\ \ (L_x^2-L_y^2),\\
V(T_2\alpha\beta) &= 1/\sqrt{2}\ \ (L_\alpha L_\beta+L_\beta L_\alpha).
\end{aligned} \tag{8}$$

The corresponding tensors for trigonal symmetry are

$$\begin{aligned}
V(Eu_\pm) &= \mp 1/\sqrt{2}\ [V(Eu)\pm iV(Ev)],\\
V(T_2x_0) &= 1/\sqrt{3}\ [V(T_2yz)+V(T_2xz)+V(T_2xy)],\\
V(T_2x_\pm) &= \mp 1/\sqrt{3}\ [\omega^{\pm}V(T_2yz)+\omega^{\mp}V(T_2xz)\\
&\qquad +V(T_2xy)],
\end{aligned} \tag{9}$$

where $\omega^{\pm}=-1/2\pm i\sqrt{3}/2$.

The matrix of the Zeeman Hamiltonian (Eq. 7) with the trigonal basis [Eq. (5)] is given in Table I. The explicit forms of the g values in terms of the effective first and second order g values in Eq. (7) are given in Table II. The latter can be expressed in terms of the basic one-electron ligand field

TABLE II. Second order g values for a $^2T_2$ multiplet in trigonal symmetry.[a]

g_{z1}	$g_1-2K_z-1/(3\sqrt{3})g_3$
g_{z1}'	$-\frac{1}{3}g_2+\frac{\sqrt{6}}{9}g_3$
g_{z2}	$c^2(\theta)\left(g_1+2\frac{\sqrt{3}}{9}g_3\right)+s^2(\theta)\left(-g_1-2K_z+\frac{\sqrt{3}}{9}g_3\right)$ $+s(2\theta)\left(-\frac{1}{3}g_2-\frac{\sqrt{3}}{18}g_3\right)$
g_{z23}	$s(2\theta)\left(g_1+K_z+\frac{\sqrt{3}}{18}g_3\right)+c(2\theta)\left(\frac{1}{3}g_2+\frac{\sqrt{3}}{18}g_3\right)$
g_{x12}'	$c(\theta)(1/(3\sqrt{2})g_2-1/(3\sqrt{3})g_3)+s(\theta)(\frac{1}{6}g_2-1/(3\sqrt{6})g_3)$
g_{x12}''	$c(\theta)(-\frac{1}{6}g_2-1/(6\sqrt{3})g_3-\sqrt{2}K_x)+s(\theta)(g_1+1/(6\sqrt{3})g_3)$
g_{x2}	$c^2(\theta)(g_1-1/(3\sqrt{3})g_3)+s^2(\theta)(-1/(3\sqrt{2})g_2-2/(3\sqrt{3})g_3)$ $+s(2\theta)\left(-\sqrt{2}K_x+\frac{1}{6}g_2+\frac{\sqrt{6}}{36}g_3\right)$
g_{x23}	$s(2\theta)\left(\frac{1}{2}g_1+\frac{\sqrt{2}}{12}g_2+\frac{\sqrt{3}}{18}g_3\right)-c(2\theta)\left(-\sqrt{2}K_x+\frac{1}{6}g_2+\frac{\sqrt{6}}{36}g_3\right)$

[a]$c(\theta)=\cos(\theta)$, $s(\theta)=\sin(\theta)$, $c^2(\theta)=\cos^2(\theta)$, and so on. The expressions for $g_{\alpha 3}$ and g_{x13} are obtained from $g_{\alpha 2}$ and g_{x12} by replacing $c(\theta)$ by $s(\theta)$ and $s(\theta)$ by $-c(\theta)$. For all cases $g_x=g_y$.

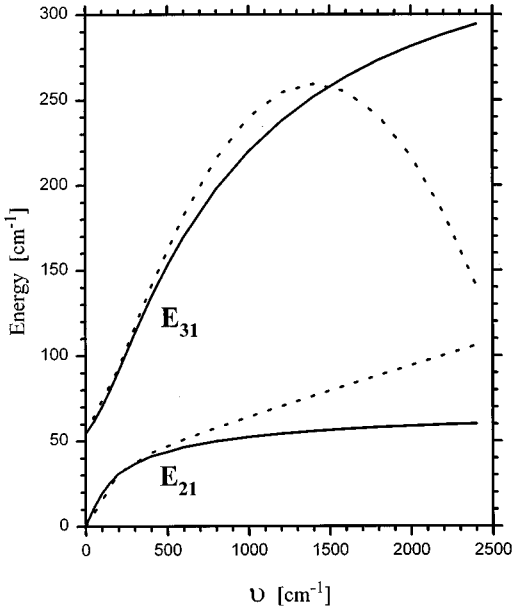

FIG. 2. Comparison between the transition energies E_{21} and E_{31} obtained from exact diagonalization of $T_2 \otimes e$ coupling (solid lines) and the corresponding energies obtained from Hams perturbation model (dotted lines). [See Eqs. (12a) and (12b) in Ref. 11.] The parameters used were $\Delta = 19\,500$ cm^{-1}, $\upsilon' = 0$, $\zeta = \zeta' = 120$ cm^{-1}, $k = k' = 0.8$, $\hbar\omega = 450$ cm^{-1}, $E_{\mathrm{JT}} = 336$ cm^{-1}.

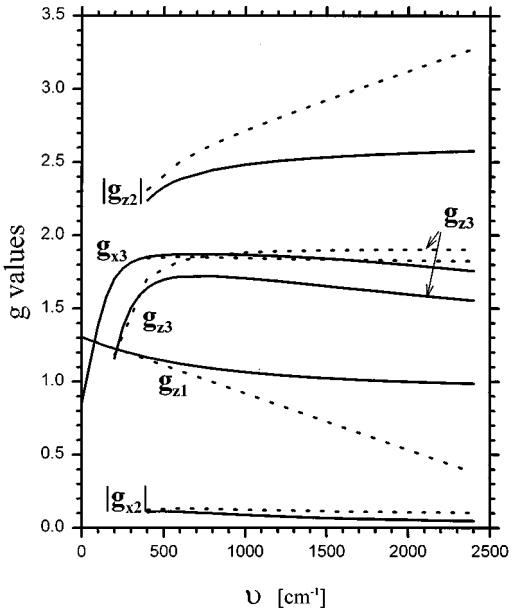

FIG. 3. Comparison between the g values of the three lowest vibronic levels for $T_2 \otimes e$ coupling which were obtained by exact diagonalization (solid lines) and from perturbation formulae (dotted lines) given in Eq. (10) and Table II. The parameters g_{z2} and g_{x2} have negative signs. The parameters g_{z2}, g_{z3} and g_{x2} change sign for small values of υ but this behavior was omitted for clarity. The ligand field parameters are the same as in Fig. 1.

parameters. Stevens has gone further and determined the explicit forms in the presence of $T_2 \otimes e$ coupling, but for small υ. If we transform his results into our parametric scheme [Eq. (7)] then we obtain,

$$
\begin{aligned}
g_1 &= 2 - 8k'\zeta'/(3\Delta) - 4k\zeta f_b/(3\hbar\omega), \\
g_2 &= -8\sqrt{2}k'\zeta'/\Delta + 2\sqrt{2}k\zeta f_b/\hbar\omega, \\
g_3 &= 4\sqrt{3}k'\zeta'\gamma/\Delta + 2\sqrt{3}k\zeta f_a/\hbar\omega, \\
K_z &= k\gamma - 2\sqrt{2}\upsilon' k'\gamma/\Delta + 2\upsilon k f_a/(3\hbar\omega), \\
K_x &= k\gamma + \sqrt{2}\upsilon' k'\gamma/\Delta - \upsilon k f_a/(3\hbar\omega),
\end{aligned}
\tag{10}
$$

where γ, f_a, f_b are the standard Ham reduction factors[11,12] for Jahn–Teller coupling to a single mode of e symmetry and frequency $\hbar\omega$. Equation (10) reduces to the static ligand field model by setting $\gamma = 1$, $f_a = 0$, $f_b = 0$.

Figure 2 compares the transition energies obtained from the Ham model and from the exact calculation as υ increases. Similarly, the approximate $g_{\parallel}$ and $g_{\perp}$ values obtained from Table II and Eq. (10) are compared with the exact values in Fig. 3.

The agreement between the two calculations is almost exact for υ in the range 0 to 400 cm^{-1} and the differences remain small for υ approaching 800 cm^{-1}. Beyond $\upsilon = 1000$ cm^{-1} the errors in the approximate g_{z1} and E_{21} values increase almost linearly with υ. It is therefore not surprising that the Ham model works very well for Ti^{3+}:Al_2O_3 where $\upsilon = 700$ cm^{-1}. On the other hand, for β alums where $\upsilon > 1500$ cm^{-1} it is essential to diagonalize the $T_2 \otimes e$ coupling exactly in order to obtain accurate values for E_{21} and g_{z1}.

III. THE $g_{\perp}$ VALUES FOR $\phi_1(2\Gamma_6)$ IN TRIGONAL SYMMETRY

If υ has a positive sign then the lowest level of the $^2T_2$ multiplet will always be $\phi_1(2\Gamma_6)$ with $g_{\perp}(2\Gamma_6) = 0$, in the presence or absence of Jahn–Teller coupling. However, it is possible to generate a nonvanishing $g_{\perp}$ in the limiting case where the energy gap, E_{21}, is very small and comparable to the Zeeman energy in an EPR experiment. This limit can be achieved if the Jahn–Teller coupling is sufficiently large.

We have investigated this problem for the case of Ti^{3+}:Al_2O_3 by varying the vibronic coupling while keeping all other parameters constant. Increasing the vibronic coupling constant, A_1, is equivalent to increasing the Jahn–Teller stabilization energy through the relation $A_1 = [E_{\mathrm{JT}}\hbar\omega]^{1/2}$. We found that even if E_{JT} was raised to 600 cm^{-1} the calculated energy gap, $E_{21} = 3.2$ cm^{-1}, was still too large to generate any significant $g_{\perp}$ in the ground state.

The magnitude of E_{JT} is restricted by the weak antibonding energy of the t_2 orbitals[24] and the typical values of E_{JT} that have been used for the Ti^{3+} ion are $E_{\mathrm{JT}} = 200$ cm^{-1} and $\hbar\omega = 200$ cm^{-1} for Ti^{3+}:Al_2O_3,[11] and $E_{\mathrm{JT}} = 320$ cm^{-1} and $\hbar\omega = 258$ cm^{-1} for Ti^{3+}:$LiNbO_3$.[14] Similar results are expected for CsTiS alum and we conclude that for any realistic value of Jahn–Teller coupling, $E_{\mathrm{JT}} < 600$ cm^{-1}, it is impossible to account for the observed $g_{\perp} = 1.14$ if the symmetry is trigonal and υ is positive. Therefore, the trigonal symmetry of the $Ti(H_2O)_6^{3+}$ ions must be removed in the low temperature form of CsTiS.

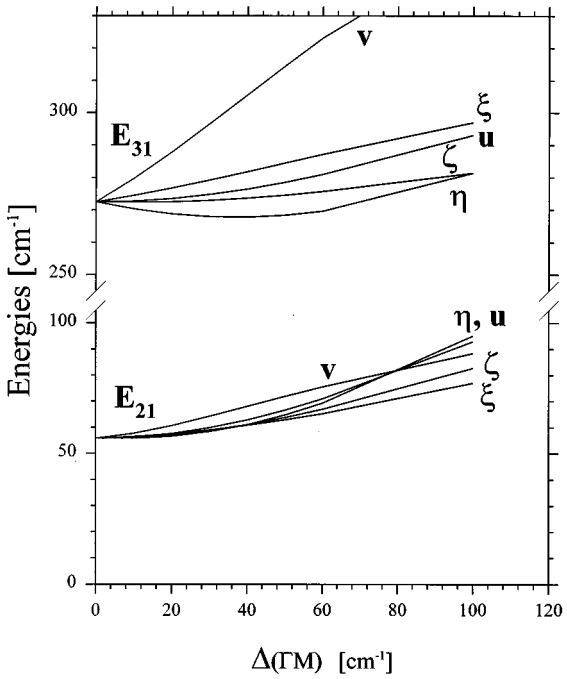

FIG. 4. The dependence of the transition energies E_{31} and E_{21} on distortions with symmetry Eu, Ev, T_2yz, T_2xz, and T_2xy, abbreviated as u, v, ξ, η and ζ, respectively. The parameters are the same as in Fig. 1 with $v=1800$ cm^{-1}.

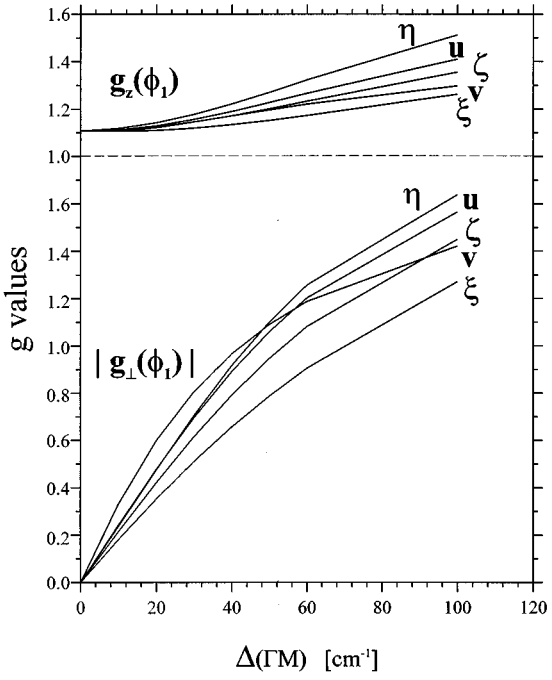

FIG. 5. The effect of distortions on the g values of the ground Kramers doublet $\phi_1(2\Gamma_6)$. The parameters are the same as in Fig. 1 with $v=1800$ cm^{-1}.

IV. $^2T_2$ COUPLING AND LOW SYMMETRY POTENTIALS

The direct product $t_2\times t_2=a_1+e+[t_1]+t_2$ shows that all the low symmetry distortions of the $^2T_2$ multiplet can be described by five real cubic tensors $V(\Gamma M)$ [see Eq. (8)]. The matrices of $V(\Gamma M)$ with the complex trigonal basis given in Eq. (5) were incorporated into the dynamic Jahn–Teller calculation. The effect of the low symmetry distortions on the transition energies and the g values of the lowest set of vibronic levels are displayed in Figs. 4–6, where $\Delta(\Gamma M)$ is the coefficient of the operator $V(\Gamma M)$ and gives a measure of the one-electron splitting of the t_2 orbitals. For example, $\Delta(Eu)=(-\sqrt{6}/3)\Delta(t_2)$, where $\Delta(t_2)=E(t_2xy)-E(t_2xz,yz)$ is the standard one-electron tetragonal splitting.[25]

The $T_2\otimes e$ calculations were made with the following ligand field parameters: $\Delta=19\,500$ cm^{-1}, $\zeta=120$ cm^{-1}, $v=1800$ cm^{-1}, $v'=250$ cm^{-1}, $k=0.75$, $k'=k$ and $\zeta'=\zeta$. The v' parameter was obtained by fitting the ligand field model to the zero field splitting of the ground state of CsCrS (see Ref. 26) and v was deduced from the effective trigonal field observed in the electronic Raman of CsVS (see Ref. 16) where $v+2/3v'\sim2000$ cm^{-1}. The active Jahn–Teller mode was assumed to be the skeletal $Q(E)$ vibration with an energy of 450 cm^{-1} (see Refs. 27 and 28) and $E_{\rm JT}$ was varied to give a rough agreement with the $g_\parallel$ value for CsTiS and was finally fixed at $E_{\rm JT}=336$ cm^{-1}.

Figure 4 shows that the $^2T_2$ multiplet with $T_2\otimes e$ coupling and large positive v is characterized by a low lying excited state at $E_{21}=56$ cm^{-1} and a higher lying state at $E_{31}=273$ cm^{-1}. The transition energies increase slowly with increasing strain. In this work we will examine more closely the effect of strain on the g values, illustrated in Figs. 5 and 6.

Figure 5 shows that a very small strain of any symmetry induces into the ground state level a $g_\perp$ that varies linearly with $\Delta(\Gamma M)$ and is described by the second order perturbation

$$g_\perp(\phi_1)\cong 2[\Delta(\Gamma M)/E_{21}]\langle\phi_{1+}x|V(\Gamma M)|\phi_{2-}\rangle \times\langle\phi_{2-}|x''_{12}|\phi_{1-}\rangle. \quad (11)$$

As $\Delta(\Gamma M)$ becomes comparable to E_{21}, Eq. (11) is no longer accurate. For the case $\Gamma M=Eu$ and T_2xy the variation of $g_\perp(\phi_1)$ can be very accurately described by a 2×2 matrix involving ϕ_1 and ϕ_2 levels. This perturbation model is less accurate for strains of other symmetry where evidently the strain coupling to ϕ_3 is larger. The basic mechanism for inducing $g_\perp(\phi_1)$ remains essentially the same for all cases and we consider in more detail the simple case of strain with Eu symmetry.

The invariance of $g(\phi_3)$ values to $\Delta(Eu)$ (Fig. 6) indicates that the strain mixing of ϕ_3 with ϕ_1 and ϕ_2 is very small. Consider the 2×2 matrix for the $\phi_{1\pm}$ and $\phi_{2\mp}$ basis with diagonal energies 0 and E_{21}, respectively. By applying this model to the numerical output we deduce, $g''_{x12}=1.951$ and $\langle\phi_{1\pm}|V(Eu)|\phi_{2\mp}\rangle=0.35$ in units of $\Delta(Eu)$.

The calculated g values in strict trigonal symmetry are $g_{z1}=1.108$, $g_{z2}=-2.505$, $g_{z3}=1.665$, $g_{x2}=-0.057$, $g_{x3}=1.828$. These can be compared with the approximate values obtained from Eq. (10) and Table II by taking $\theta=87.2°$ [Eq. (6)]: $g_{z1}=0.71$, $g'_{z1}=-0.04$, $g_{z2}=-2.96$, $g_{z3}=1.90$, g_{x2}

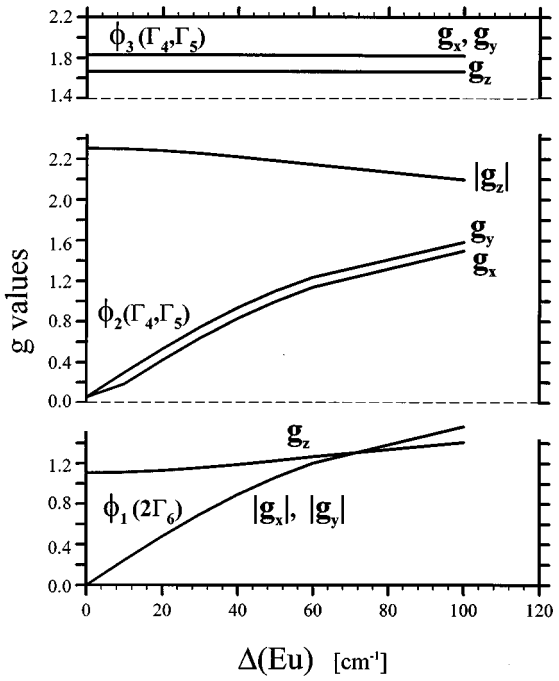

FIG. 6. The effect of $V(Eu)$ distortion on the g values of the three lowest vibronic states in the $T_2\otimes e$ model. The parameters are the same as in Fig. 1 with υ=1800 cm^{-1}.

$=-0.10$, $g_{x3}=1.84$ and $g''_{x12}=1.86$. Furthermore, Eq. (10) and Table II give $g'_{x12}=0.02$, $g'_{x13}=0.03$, $g''_{x13}=-0.26$, $g_{x23}=0.02$ and $g_{z23}=0.15$. The second order equations evidently give the correct signs and even useful estimates of the g values. Clearly, the most important Zeeman matrix element is the off-diagonal g''_{x12} which is always large because it contains a large contribution from g_1 that is not quenched by the Jahn–Teller coupling.

If the low symmetry perturbation is diagonalised with the basis $\phi_{1\pm}$ and $\phi_{2\pm}$

$$\begin{aligned}\overline{\phi_{1\pm}}&=c_2\phi_{1\pm}-c_1\phi_{2\mp},\\ \overline{\phi_{2\pm}}&=c_1\phi_{1\pm}+c_2\phi_{2\mp},\end{aligned}\tag{12}$$

where $c_2>c_1$ and c_2 is given a positive sign then for the two lowest levels we obtain

$$\begin{aligned}\overline{g_{z1}}&=c_2^2g_{z1}-c_1^2g_{z2},\\ \overline{g_{z2}}&=c_1^2g_{z1}-c_2^2g_{z2},\\ \overline{g_{x1}}&=-2c_1c_2g_{x12}+c_1^2g_{x2},\\ \overline{g_{y1}}&=-2c_1c_2g_{x12}-c_1^2g_{x2},\\ \overline{g_{x2}}&=2c_1c_2g_{x12}+c_2^2g_{x2},\\ \overline{g_{y2}}&=2c_1c_2g_{x12}-c_2^2g_{x2},\end{aligned}\tag{13}$$

where $g_{xi}=g_{yi}$ and g_{x12} is to be identified with g''_{x12}. Actually, g_{x12} includes the small contribution of g'_{x12} because the full 4×4 matrix for the ϕ_1 and ϕ_2 subspace as given in Table I can always be transformed into 2×2 matrices.

We now see that the anisotropy in the induced $g_\perp$ of the ground state is $2c_1^2g_{x2}$ and is very small because c_1^2 is very small. The condition for inducing an apparent axial $g_\perp$ into a Kramers doublet is that $g_\perp\sim0$ in exact axial symmetry and that the doublet is coupled to another Kramers doublet by both strain and by an axial off-diagonal Zeeman term.

The ϕ_2 level has $g_\perp=g_{x2}$ in exact trigonal symmetry. In this case, the anisotropy in the apparent $g_\perp(\phi_2)$ is $2c_2^2g_{x2}$ that is approximately constant since c_2^2 varies from 1.00 to 0.811 as $\Delta(Eu)$ varies from 0 to 100 cm^{-1} (Fig. 6).

V. SOME APPLICATIONS

Figure 5 shows that $g_\perp(\phi_1)$ is a sensitive detector of strain of any symmetry. The previous analysis (Sec. IV) can be applied with very little modification to all $(t_2^1)\ ^2T_2$ multiplets that have a positive axial field, υ or $\Delta(t_2)$, of any magnitude. Table III lists a number of examples which display a range of low symmetry distortions.

The nonvanishing $g_\perp$ for Ti^{3+}:Al_2O_3 has already been attributed to lattice strains but a detailed investigation of a microscopic mechanism was not pursued.[21] If we represent the distortion by $V(Eu)$ then the observed $g_\perp\sim0.14$ requires $\Delta(Eu)\sim4$ cm^{-1}.

The g values of CsTiS can be fitted with $\Delta(Eu)\sim56$ cm^{-1}. In Fig. 6 the curves for $g_z(\phi_1)$ and $g_\perp(\phi_1)$ cross at $\Delta(Eu)\sim70$ cm^{-1} where the g values are predicted to have the value 1.31, in good agreement with the isotropic value observed for deuterated[29] CsTiS (Table III).

TABLE III. Strain induced $g_\perp$ for the $^2T_2$ (ϕ_1) Kramers doublet with positive υ.[a]

	Experimental			Calculated	
	$g_\parallel$	$g_\perp$	Ref.	$\Delta(Eu)$[b]	$g_\parallel$[b]
Ti^{3+}:Al_2O_3	1.07	~0.14	21	4.1	1.07
Ti^{3+}:$CsAl(SO_4)_2\cdot12H_2O$	1.17	0.23	33	10	1.11
	1.19	0.70		30	1.16
	1.24	0.93		43	1.20
$CsTi(SO_4)_2\cdot12H_2O$	1.25	1.14	3	56	1.25
$CsTi(SO_4)_2\cdot12D_2O$	1.31	1.31	29	70	1.31
Ti^{3+}:$NH_3CH_3Al(SO_4)_2\cdot12H_2O$	1.40	1.61	32	110	1.44

[a]ϕ_1 transforms as $M_J=\pm\frac{3}{2}$ for $J=\frac{3}{2}$.
[b]The observed $g_\perp$ was used to estimate $\Delta(Eu)$ in cm^{-1} (Fig. 5), which was then used to predict $g_\parallel$, given in the last column. Separate calculations were made for Ti^{3+}:Al_2O_3.

NH_3CH_3AlS is a β alum that has a ferroelectric transition at 177 K where the cubic space group changes to $Pca2_1$. Low symmetry ligand fields are indicated by the EPR of Cr^{3+}:NH_3CH_3AlS, measured below 177 K.[31] All β alums have large and positive v. Accordingly, the previous analysis[23,32] of the EPR and spin-lattice relaxation rates of Ti^{3+}:NH_3CH_3AlS have to be corrected.

The g values of Ti^{3+}:NH_3CH_3AlS measured below 5 K (Table III) can be fitted to an arbitrary $V(Eu)$ strain. The observed $g_\perp = 1.61$ requires $\Delta(Eu) \sim 110\ cm^{-1}$ and $g_\parallel$ is predicted to be 1.44, in fair agreement with the observed $g_\parallel = 1.40$.

Two features in the earlier work on Ti^{3+}:NH_3CH_3AlS may be important. Firstly, the spin-relaxation time has a large dependence on the direction of the applied magnetic field.[23] The relaxation time is a maximum when B lies along the [111] direction and drops sharply as B deviates away from the [111] direction. In contrast to the earlier analysis, we suggest that the orbit-lattice interaction and the off-diagonal Zeeman term (x''_{12} in Table I) provide the most efficient second-order amplitude for the angular dependence of the spin-lattice relaxation time.

This suggestion lends support to the earlier interpretation[33] of the EPR of Ti^{3+}:CsAlS. In this case the EPR shows fine structure spread over ~300 gauss and has been interpreted to consist of at least three distinct chemical species with apparent axial symmetry. ''The intensity of the lines decreased very rapidly as the magnetic field diverges from the direction of the cube diagonal.'' [33] If we use the reported $g_\perp$ to fix the value of $\Delta(Eu)$ then the predicted $g_\parallel$ will correspond closely to the empirical $g_\parallel$ values (Table III).

The second feature of the EPR of Ti^{3+}:NH_3CH_3AlS is that the reported line width of ~20 gauss[32] is much smaller than the value of 250 gauss observed for CsTiS. The latter value is much larger than that expected for pure magnetic dipole interaction.[3] It seems possible that just as for Ti^{3+}:CsAlS, the EPR of CsTiS may consist of several unresolved chemical species with different low symmetry fields. Such details will require precise information on the crystal structure at low temperatures.

In the analysis of the data in Table III we have used an arbitrary distortion of Eu symmetry. In all cases the ground state is $^2T_2$ (^2E) and is subject to a Jahn–Teller distortion. The direct product of the trigonal species E requires the distorting potentials to be of $Eu_\pm$ and $T_2x_\pm$ symmetry in the parent cubic symmetry [Eq. (7)]. The large trigonal field v stabilises the (t_2^1) ^2E state and it is unlikely that the distortions will be of $Eu_\pm$ type, which involve compression and elongation of the strong sigma M–O bonds and tend to destroy the v trigonal field. Rather, the distortions should be of $T_2x_\pm$ symmetry, which involve the lower-energy bending or angular distortions of M–O bonds. Therefore, it is not surprising that the $\Delta(Eu)$ parameters in Table III are very small. Furthermore, Fig. 4 suggests that the dependence of $g_{x,y}(\phi_1)$ on T_2yz, T_2xz, T_2xy and hence on $T_2x_\pm$ potentials [Eq. (9)], may be represented empirically by an effective or average operator $V(Eu)$.

VI. CONCLUSIONS

The low temperature paramagnetic properties of CsTiS are largely determined by the two lowest vibronic levels that are coupled by a large trigonal Zeeman term that operates in the direction perpendicular to the molecular trigonal axis. This off-diagonal Zeeman term should make the spin-lattice relaxation time sharply dependent on the direction of the applied magnetic field and can be easily induced into both the ground and excited vibronic levels by small low-symmetry distortions.

[1] J. Sygusch, Acta Crystallogr. **B30**, 662 (1974).
[2] D. Bijl, Proc. Phys. Soc. London **A63**, 405 (1950).
[3] B. Bleaney *et al.*, Proc. Phys. Soc. London **A68**, 57 (1955).
[4] A. Bose, A. S. Chakravarty, and R. Chatterjee, Proc. R. Soc. London Ser. A **255**, 145 (1960).
[5] A. Manoogian, Can. J. Phys. **48**, 2577 (1970).
[6] G. F. Dionne, Can. J. Phys. **50**, 2232 (1972).
[7] Y. H. Shing and D. Walsh, Phys. Rev. Lett. **33**, 1067 (1974).
[8] G. F. Dionne, Can. J. Phys. **42**, 2419 (1964).
[9] S. Sugano, Y. Tanabe, and H. Kamimura, *Multiplets of Transition Metal Ions in Crystals* (Academic, New York, 1970).
[10] G. F. Koster *et al.*, *Properties of the Thirty-two Point Groups* (MIT, Cambridge, MA, 1963).
[11] R. M. Macfarlane, J. Y. Wong, and M. D. Sturge, Phys. Rev. **166**, 250 (1968).
[12] F. S. Ham, Phys. Rev. **138**, A1727 (1965).
[13] R. Ameis, S. Kremerand, and D. Reinen, Inorg. Chem. **24**, 2751 (1985).
[14] O. Thiemann *et al.*, Phys. Rev. B **49**, 5845 (1994).
[15] C. Daul and A. Goursot, Inorg. Chem. **24**, 3554 (1985).
[16] S. P. Best and R. J. H. Clark, Chem. Phys. Lett. **122**, 401 (1985).
[17] M. Brorson and M. Gajhede, Inorg. Chem. **26**, 2109 (1987).
[18] S. P. Best and J. B. Forsyth, J. Chem. Soc. Dalton Trans. 3507 (1990).
[19] S. P. Best and J. B. Forsyth, J. Chem. Soc. Dalton Trans. 1721 (1991).
[20] S. P. Best, J. B. Forsyth, and P. L. Tregenna-Piggott, J. Chem. Soc. Dalton Trans. 2711 (1993).
[21] C. A. Bates and J. P. Bentley, J. Phys. C **2**, 1947 (1969).
[22] M. Abou-Ghantous, C. A. Bates, and K. W. H. Stevens, J. Phys. C **7**, 325 (1974).
[23] Y. H. Shing, C. Vincent, and D. Walsh, Phys. Rev. Lett. **31**, 1036 (1973).
[24] M. Bacci, Chem. Phys. **40**, 237 (1979).
[25] J. Glerup and C. E. Schaeffer, in *Progress in Coordination Chemistry*, edited by M. Cais (Elsevier, Amsterdam, 1968), p. 500.
[26] A. G. Danilov, J. C. Vial, and A. Manoogian, Phys. Rev. B **8**, 3124 (1973).
[27] S. P. Best, R. S. Armstrong, and J. K. Beattie, J. Chem. Soc. Dalton Trans. 1655 (1982).
[28] S. P. Best, J. K. Beattie, and R. S. Armstrong, J. Chem. Soc. Dalton Trans. 2611 (1984).
[29] B. V. Harrowfield, Phys. Abstr. **75**, 594 (1972).
[30] R. O. W. Fletcher and H. Steeple, Acta Crystallogr. **17**, 290 (1964).
[31] D. W. O'Reilly and Tung Tsang, Phys. Rev. **157**, 417 (1967).
[32] Y. H. Shing, C. Vincent, and D. Walsh, Phys. Rev. B **9**, 340 (1974).
[33] G. A. Wooton and J. A. MacKinnon, Can. J. Phys. **46**, 59 (1968).